Compressive deformation of a single microcapsule

K. K. Liu,* D. R. Williams, and B. J. Briscoe
Department of Chemical Engineering, Imperial College of Science, Technology and Medicine, London SW7 2BY, United Kingdom
(Received 12 March 1996)

This paper reports an experimental and theoretical study of the compressive behavior of single microcapsules; that is, liquid-filled cellular entities (approximately 65 μm in diameter) with a thin polymeric membrane wall. An experimental technique which allows the simultaneous measurement of both the compressive displacement and the reaction forces of individual microcapsules deformed between two parallel plates up to a dimensionless approach [(compressive displacement)/(initial particle diameter)] of 60% is described. The corresponding major geometric parameters of the deformed microcapsule, such as central lateral extension as well as the failure phenomena, are reported and recorded through a microscopic visualization system. The elastic modulus, the bursting strength of the membrane, and the pressure difference across the membrane are computed by using a theoretical analysis which is also presented in this paper. This theoretical model, which was developed by Feng and Yang [J. Appl. Mech. **40**, 209 (1973)] and then modified by Lardner and Pujara [in *Mechanics Today*, edited by S. Nemat-Nasser (Pergamon, New York, 1980), Vol. 5], considers the deformation of a nonlinear elastic spherical membrane which is filled with an incompressible fluid. The predictions of the theory are consistent with the experimental observations. [S1063-651X(96)05011-8]

PACS number(s): 87.22.−q, 68.45.−v, 07.10.Cm

I. INTRODUCTION

Microcapsules, that is, liquid-filled cells with thin membrane walls, are now used in the pharmaceutical, agriculture, and food industries, as well as in biotechnology industries for a wide range of applications from drug delivery to the construction of synthetic cells for artificial organs and artificial blood. The mechanical properties of these synthetic microcapsules have been recognized as being important not only for determining the kinetics of the release of encapsulated chemicals but also for controlling the durability of the products during processing and in use. The process of compacting microcapsules via compression is considered as a convenient method for assembling microcapsule particles into a dosage form. However, the individual particles must exhibit sufficient physical integrity in order to withstand processing while maintaining the required drug release profile in their final dosage form [1]. Moreover, some studies [2,3] have shown the pressure difference across the wall membrane may be one of the critical factors which affects the rate of drug release from tableted microcapsules. In addition, deformable liquid-filled microcapsules exist pervasively in natural biological systems in many and various forms. Some authors [4] consider the mammalian red blood cell motion in the microcirculation environment to be analogous to the squeezing of liquid-filled membrane systems between two parallel plates.

There are several experimental methods which have been reported for characterizing the deformation behavior of microcapsules. Jay and Edwards [5] have measured the elastic properties of the membrane of microcapsules by using the micropipette aspiration technique. Chang and Olbricht [6] have studied the elastic properties of the membrane by observing the motion and deformation of a synthetic, liquid-filled capsule (diameter about 2 to 4 mm) that was freely suspended in a hyperbolic extensional flow. However, this method has not been applied to microcapsules. Recently, Zhang, Saunders, and Thomas [7] have measured the bursting strength of microcapsules by using a micromanipulation technique which squeezes a single microcapsule between two platens. Since the relative position of the moving platens cannot be accurately determined by this route, a detailed study of the deformation behavior of the microcapsules is currently difficult using this method.

A suitable experimental technique and associated theoretical models which permit the simultaneous study of the elasticity, the tension distribution and bursting strength of the microcapsule membrane, and the pressure difference across the membrane are reported here. The experimental technique which involves the compression of individual microcapsules between two parallel plates has been developed to directly measure the force imposed on a single microcapsule and its corresponding compressive displacement. A visual system which allows for the investigation of the corresponding major geometric deformational parameter, such as lateral extension, as well as failure phenomena has been incorporated. Through the quantitative analysis of the interrelationships between the force and the displacement, as well as the prediction of the geometric deformational parameters, the required physical information has been obtained.

Several investigators have theoretically modeled the contact mechanics of spherical nonlinear membranes. Feng and Yang [8] considered the problem of the deformations and the stresses in an inflated nonlinear elastic spherical membrane compressed between two frictionless rigid plates. Lardner and Pujara [9] extended the analysis to a membrane filled with an incompressible fluid and were able to accurately predict the deformation of the sea-urchin egg, compared with the experimental results which were previously reported by Yoneda [10]. Taber [11] has carried out experimental work

*Present address: Microsystems Laboratory, Industrial Technology Research Institute, Hsinchu, Taiwan, Republic of China.

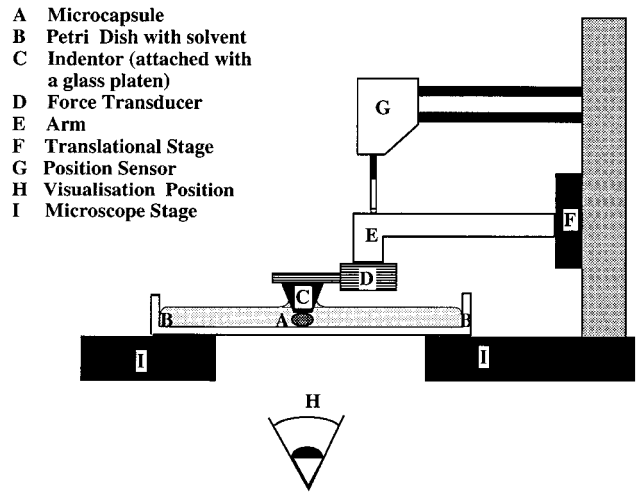

FIG. 1. The schematic view of microupsetting instrument (not to scale).

and proposed a similar theoretical model which included the wall bending moment in the governing mechanisms of the compression for fluid-filled spherical shells by rigid indenters. The present paper adapts these analyses for the interpretation of the experimental data to be described.

II. EXPERIMENT

A. Experimental arrangement

The primary functions of the instrument [12] were to provide a capability to simultaneously measure both the approach and the resultant forces, while compressing a small single sphere between parallel glass on other platens. Optical viewing of the deforming particle in a vertical plane provided a reasonable estimate of the central lateral extension of the particle and a much less accurate measurement of the contact area. The instrument system is schematically shown in Fig. 1 and is based around an inverted optical microscope (Wilovert S, Wetzlar Ltd., Germany). Attached to the microscope stage (Z plane) was a microstepper motor controlled motion stage (PTS1000, Photon Control Ltd., England) capable of discrete microsteps of less than 100 nm. A small horizontal arm on which was mounted a very sensitive force transducer (BG-10, Kulite Ltd., USA) with a force resolution better than 10^{-5} N and a maximum force capability of 10^{-1} N was attached to the motion stage. The instrument had a force and a displacement resolution of 10 μN and 0.1 μm, respectively.

On the lower face of this transducer arm was attached a small flat glass platen (2 mm diameter) for the purpose of deforming the sample. The force transducer signal was amplified and filtered using a strain gauge amplifier (369TA, Fyde Ltd., UK). The absolute position of the platen was monitored with an optically encoded displacement transducer (MT25B, Heidenhain Ltd., Germany) which resolved a vertical displacement of 100 nm over a 25 mm range. The entire instrument system was computer controlled using a purpose written software. The experiments were conducted in the temperature range 20–25 °C. The mechanical components were supported upon an antivibration table.

During all the experiments a high resolution video camera (TM 620, Pulnix Ltd., USA) connected to the microscope allowed the microcapsule diameter to be measured during the experiment.

Under large loads the cantilever beam of the force transducer may deflect sufficiently to cause a significant difference between the sensed imposed displacement and the actual imposed displacement. Routine calibration of the instruments' compliance, principally that of the force transducer, allowed the extent of this difference to be accurately determined. All the experimental load-displacement curves described in the current paper have been corrected for the deflection of the force transducer.

B. Material

The microcapsules used in this current study were a water-oil multiple emulsion drop contained within a thin polymeric membrane. The membrane wall is, in this case, made of a poly(urethane) elastomer. The diameter of the particles varied between 50 and 100 μm and the wall thickness, estimated by scanning electron microscopy following freeze fracture, ranged between 1 and 2 μm. These materials were provided by David Brown of Zeneca Ltd, U.K. Further details of their preparation are described elsewhere [13].

C. Experimental procedure

A liquid film, isotonic with the liquid contained within the microcapsules, was placed in a petri dish beneath the microscope lens. Microcapsules were randomly drawn into a micropipette and then carefully discharged into the petri dish. A particular microcapsule was chosen at random. In order to confirm that only one particle was in contact with the microplaten, the contact region was first examined using a low magnification lens on the microscope. The microplaten was then slowly driven up and down to find the initial contact point between the microplaten and the selected microcapsule. When the microplaten and the microcapsule initially touched, the microcapsule was slightly disturbed and this effect was monitored in the video image of the microcapsule shown on the video monitor. The microplaten was then driven at a constant speed, about 2 μm per second, during the microcapsule compression. The imposed force and the displacement of the squeezed microcapsule during loading and unloading were automatically recorded through the data acquisition system. Also, a video image sequence of the deformed shape of the microcapsule was recorded so that the lateral extension could be determined after the experiment. The maximum imposed displacement was gradually increased until the bursting of the microcapsule was observed.

III. THE THEORETICAL ANALYSIS

It is well known, in the elastic deformation theory of plates and shells, that the bending rigidity (D), or the flexural rigidity, of a thin isotropic plate or a thin shell is proportional to the cubic power of the wall thickness. Thus the bending rigidity may be expressed as

$$D=\frac{E\overline{h^3}}{(1-\nu^2)}, \tag{1}$$

where E is Young's modulus, $\overline{h}$ is the wall thickness, and ν is the Poisson ratio. In contrast, the extensional rigidity is Eh, and proportional to the first power of the wall thickness. When the wall thickness h is very small, the contribution to the sensed rigidity from the bending rigidity is much smaller than the contribution from the extensional rigidity [14]. Furthermore, Taber's [11] experiments and calculations for a thick shell (the ratio of radius of thickness of approximately 6.0) demonstrated that when a point load was applied the bending stress governs the behavior at small deformation (the dimensionless approach was less than 20%), but that the membrane extensional stresses dominate at larger deformations. Since the microcapsules which were used in this study have a high ratio of radius to thickness (about 16); i.e., thin wall systems, the response forces contributed from the bending moment may be reasonably neglected in the first instance. This assumption will be further discussed in Sec. IV A.

The constitutive equations (relationships between stress and strain) used in this study to represent the behavior of the microcapsules' membranes are those for Mooney-Rivlin and neo-Hookean materials which have a rubberlike nonlinear elasticity [15,16].

In the Mooney-Rivlin model the strain-energy function W^* of an isotropic incompressible material is

$$W^* = C_1(I_1-3) + C_2(I_2-3) = C_1[(I_1-3) + \beta(I_2-3)], \tag{2}$$

where C_1 and C_2 are the material constants with the dimensions of stress, $\beta = C_2/C_1$; for a homogeneous and isotropic, incompressible elastic material C_1 is equal to $6E$. I_1 and I_2 are strain invariants which may be expressed in terms of the principal stretch ratios in the meridional and circumferential directions of the deformed surface, λ_1 and λ_2, and are

$$I_1 = \lambda_1^2 + \lambda_2^2 + \frac{1}{\lambda_1^2\lambda_2^2}, \tag{3}$$

$$I_2 = \lambda_1^2\lambda_2^2 + \frac{1}{\lambda_1^2} + \frac{1}{\lambda_2^2}. \tag{4}$$

Then, the principal stresses in the meridional and circumferential directions, σ_1 and σ_2 (see below; Fig. 2), respectively, may be expressed as

$$\sigma_1 = \lambda_1 \frac{\partial W^*}{\partial \lambda_1} = 2C_1\lambda_1\lambda_2\left(\frac{\lambda_1}{\lambda_2} - \frac{1}{\lambda_1^3\lambda_2^3}\right)(1+\beta\lambda_2^2), \tag{5}$$

$$\sigma_2 = \lambda_2 \frac{\partial W^*}{\partial \lambda_2} = 2C_1\lambda_1\lambda_2\left(\frac{\lambda_2}{\lambda_1} - \frac{1}{\lambda_1^3\lambda_2^3}\right)(1+\beta\lambda_1^2). \tag{6}$$

For the configuration of this spherical membrane system, the relationship between the stress resultants per unit length of the deformed surface in the meridional and circumferential directions, T_1 and T_2, respectively, and the principal stresses σ_1, σ_2, may be expressed as

$$T_1 = \frac{h\sigma_1}{\lambda_1\lambda_2} = 2hC_1\left(\frac{\lambda_1}{\lambda_2} - \frac{1}{\lambda_1^3\lambda_2^3}\right)(1+\beta\lambda_2^2), \tag{7}$$

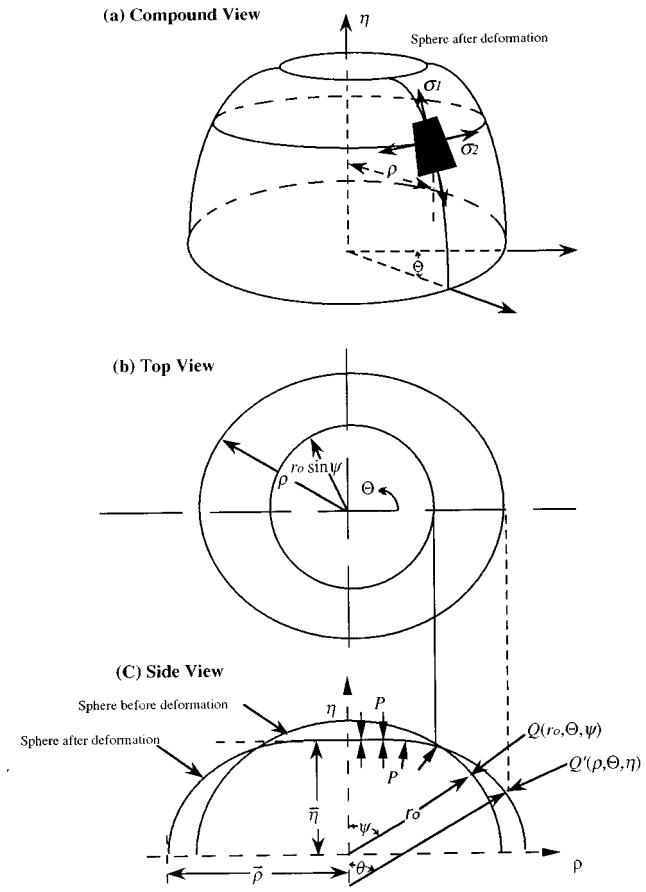

FIG. 2. Geometry for the contact problem for the half of a thin wall spherical membrane, filled with an incompressible fluid, between large rigid plates [adapted from Feng and Yang's original paper [8]]. The spherical coordinates (r_0,Θ,ψ) used for the description of the spherical membrane geometry before deformation and also cylindrical coordinates (ρ,Θ,η) which are used for the description of the deformed membrane after deformation. θ is the angle measured from the positive axis of symmetry to the outward normal of the deformed membrane surface; r_0 is the initial radius of the undeformed membrane; $\overline{\eta}$ is the distance between the rigid plate and the equator of the spherical membrane after deformation; $\overline{\rho}$ is the lateral extended radius of the deformed membrane.

$$T_2 = \frac{h\sigma_2}{\lambda_1\lambda_2} = 2hC_1\left(\frac{\lambda_2}{\lambda_1} - \frac{1}{\lambda_1^3\lambda_2^3}\right)(1+\beta\lambda_1^2), \tag{8}$$

where h is the initial thickness of the membrane.

A neo-Hookean material description may be seen as a simplification of the Mooney-Rivlin formula by assuming β is zero [16]. For a Mooney-Rivlin material the value of β has been taken, in the current study, as 0.1, as suggested by Green and Adkins [17].

Lardner and Pujara [9] derived two groups of governing equations for two separate deformation regions: the plate-membrane contact region and the non-contact deformation region. The details of the derivation of these equations are given elsewhere [8,9]. The final results for the cases shown in Fig. 2 are summarized below.

Contact region

$$\lambda_1' = \frac{\lambda_1}{\lambda_2 \sin\psi}\left(\frac{f_3}{f_1}\right) - \left(\frac{\lambda_1 - \lambda_2\cos\psi}{\sin\psi}\right)\left(\frac{f_2}{f_1}\right), \tag{9}$$

$$\lambda_2' = \frac{\lambda_1 - \lambda_2\cos\psi}{\sin\psi} \tag{10}$$

and noncontact region

$$\lambda_1' = \left(\frac{\delta\cos\psi - W\sin\psi}{\sin^2\psi}\right)\left(\frac{f_2}{f_1}\right) - \left(\frac{W}{\delta}\right)\left(\frac{f_3}{f_1}\right), \tag{11}$$

$$\delta' = W, \tag{12}$$

$$W' = \frac{\lambda_1' W}{\lambda_1} + \frac{(\lambda_1 - W^2)}{\delta}\left(\frac{T_2}{T_1}\right) - \frac{\lambda_1(\lambda_1^2 - W^2)^{1/2} Pr_0}{T_1}, \tag{13}$$

where

$$f_1 = \frac{\partial T_1}{\partial \lambda_1} = 2hC_1(1+\beta\lambda_2^2)\left(\frac{1}{\lambda_2} + \frac{3}{\lambda_1^4\lambda_2^3}\right), \tag{14}$$

$$f_2 = \frac{\partial T_1}{\partial \lambda_2} = 2hC_1\left[\left(\frac{3}{\lambda_1^3\lambda_2^4} - \frac{\lambda_1}{\lambda_2^2}\right)(1+\beta\lambda_2^2) + 2\beta\lambda_2\left(\frac{\lambda_1}{\lambda_2} - \frac{1}{\lambda_1^3\lambda_2^3}\right)\right], \tag{15}$$

$$f_3 = T_1 - T_2 = 2hC_1\left[\frac{\lambda_1}{\lambda_2} - \frac{\lambda_2}{\lambda_1} - \beta\left(\frac{1}{\lambda_1^3\lambda_2} - \frac{1}{\lambda_1^3\lambda_2^3}\right)\right], \tag{16}$$

and where P is the pressure inside the deformed membrane after contact; the primes indicate differentiation with respect to ψ, the angular position reference in the undeformed sphere; a schematic diagram of the half spherical membrane before and after contact deformation is shown in Fig. 2. The figure also shows the spherical coordinates (r_0,Θ,ψ) used for the description of the spherical membrane geometry before contact and also cylindrical coordinates (ρ,Θ,η) which are used for the description of the deformed membrane after contact. The variables δ and W are defined as

$$\delta = \lambda_2 \sin\psi, \tag{17}$$

$$W = \delta'. \tag{18}$$

The boundary conditions for this problem are

$$\psi = 0, \quad \lambda_1 = \lambda_2 = \lambda_0, \tag{19}$$

$$\psi = \Gamma, \quad (\lambda_1)_{\text{contact}} = \Gamma(\lambda_1)_{\text{noncontact}}, \tag{20}$$

$$\psi = \Gamma, \quad (\lambda_2)_{\text{contact}} = \Gamma\left(\frac{\delta}{\sin\Gamma}\right)_{\text{noncontact}}, \tag{21}$$

$$\psi = \Gamma, \quad \eta' = 0 \tag{22}$$

$$\psi = \frac{\pi}{2}, \quad \delta' = 0, \tag{23}$$

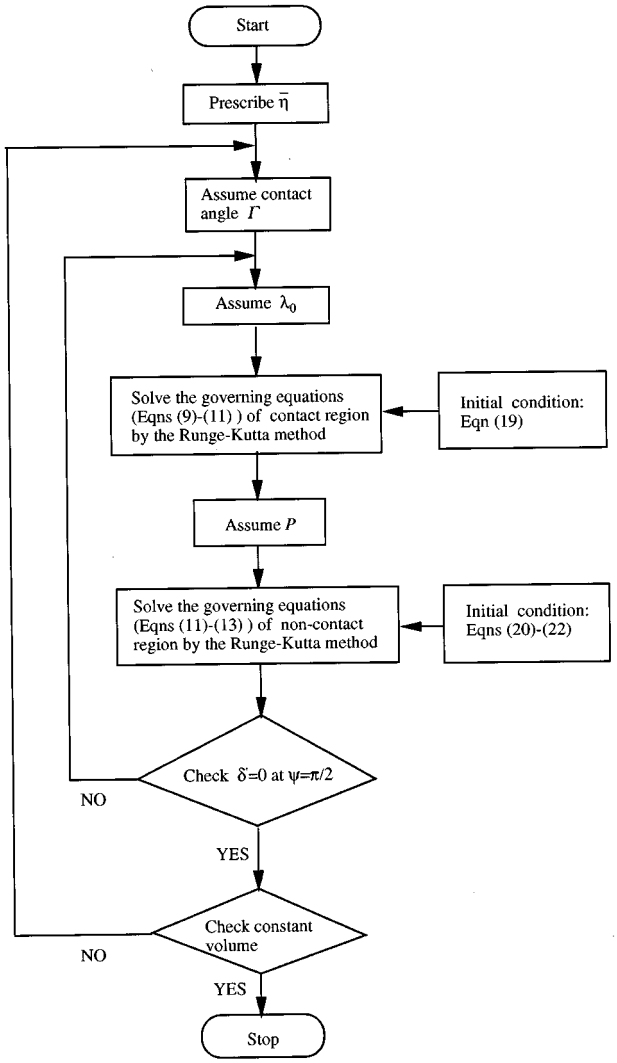

FIG. 3. The flow chart for the enhanced version of the algorithm for solving the set of equations of the membrane model used in the current study.

where Γ is the angle of the contact area; its definition is the angular position, with reference to the undeformed membrane, which is measured from the positive axis of symmetry to the boundary between the contact region and the noncontact region after deformation [8].

Since the original boundary-value problem has been transformed into an initial value problem, the governing equations [Eqs. (9)–(13)], with their boundary conditions, can be solved by a standard numerical scheme, the Runge-Kutta method [18]. Extending the works of Feng and Yang [8] and Lardner and Pujara [9], an independent computer algorithm was developed as described in Fig. 3. The calculation procedures of Feng and Young and Lardner and Pujara both prescribed the angle of contact area (Γ) and then calculated the other parameters which included the distance between the rigid plate and the equator of the spherical membrane after contact, $\bar{\eta}$ (see Fig. 2). However, the angle of the contact area has been proven to be difficult to measure accurately by direct experimental observation in these microscopic systems [10]. Hence it is appropriate to modify their procedures so as to prescribe $\bar{\eta}$ and then to calculate the

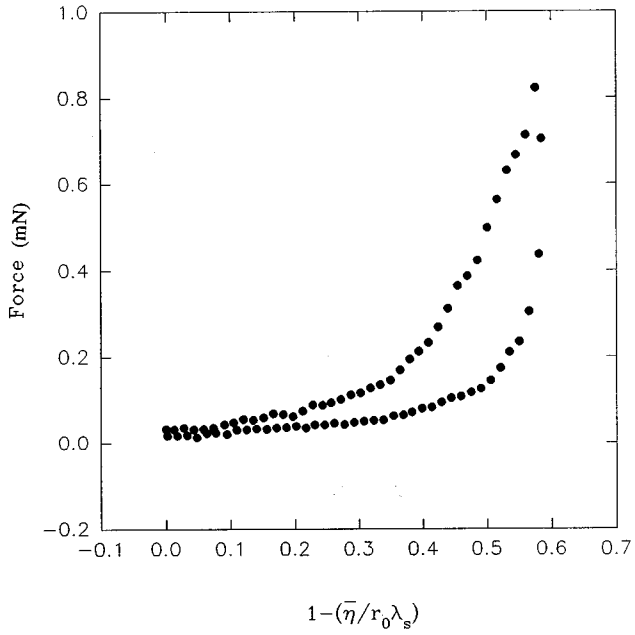

FIG. 4. The experimental loading and unloading (after bursting) curve of the 65 μm microcapsule. The bursting point is near 58% dimensionless approach α [$=1-(\overline{\eta}/r_0\lambda_s)$].

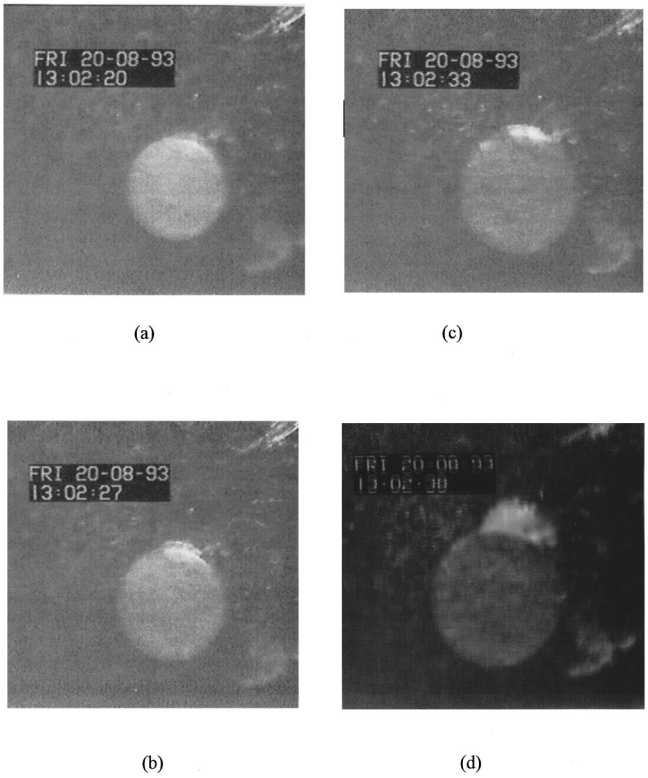

FIG. 5. Photographs of the bottom view of the deformed microcapsule (approximately 65 μm in diameter) for various dimensionless approaches α; (a) α=0%, (b) α=20%, (c) α=40%, (d) α=58%.

other parameters. The assumption, suggested by Lardner and Pujara, that the volume of encapsulated solution is constant has been adopted in the current analysis. The flow chart of the algorithm, applied in the current study, is presented in Fig. 3.

IV. RESULTS AND DISCUSSIONS

The above theoretical analysis, combined with the corresponding experimental data, provides a route for determining the elastic modulus of the membrane (Sec. IV A), the internal pressure (Sec. IV B), the tension distribution on the membrane (Sec. IV C), and the geometric features of the deformation (Sec. IV D). By a comparison with the experimental observations, the basic assumptions adopted in the theory, outlined above, may be tested.

A. Elastic modulus of the membrane

The loading-unloading curve for a 65 μm microcapsule up to a 60% deformation [dimensionless approach; (compressive displacement)/(initial diameter)] has been investigated and is shown in Fig. 4. The dimensionless approach parameter (α) comprises the distance between the rigid plate and the equator of the spherical membrane after contact, $\overline{\eta}$, the stretch ratio of the initial inflation, λ_s, and the radius of the undeformed microcapsule, r_0, and is of the form $1-(\overline{\eta}/r_0\lambda_s)$ [9]. Since in our case the liquid in the petri dish was isotonic with the liquid contained in the microcapsules, it is reasonable to assume that the initial inflation is zero; i.e., that $\lambda_s=1$, although this condition is unproven. Based upon optical observations during the loading process, the microcapsule started to burst when the deformation reached about a value of 58% deformation [see Fig. 5(d)]. The unloading curve, after the burst, shows that the reaction force is now

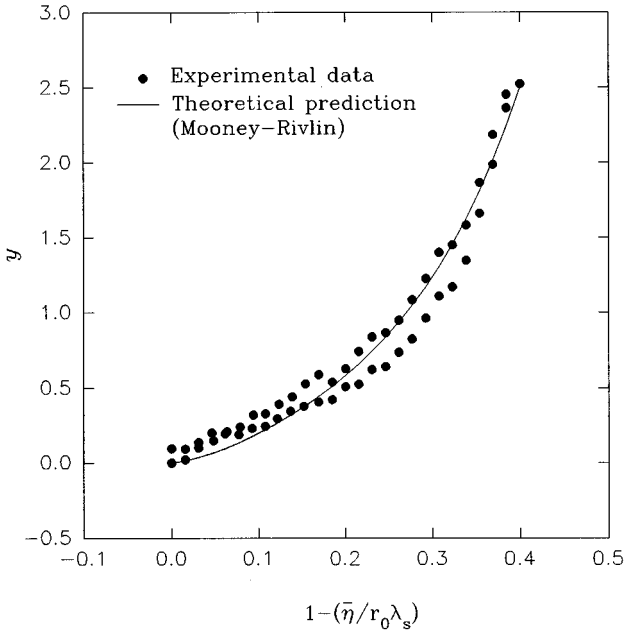

FIG. 6. The dimensionless experimental loading-unloading curve (deformation up to 40%) and theoretical predictions by the membrane model with the Mooney-Rivlin material law. The parameter $y=(F/C_1hr_0\lambda_s^2)$ is the dimensionless force and the quantity $1-(\overline{\eta}/r_0\lambda_s)$ is the dimensionless approach. λ_s is 1.0 and C_1 is 16.08 MPa. The wall thickness (h) is taken as 2 μm. The material constant β is taken as 0.1.

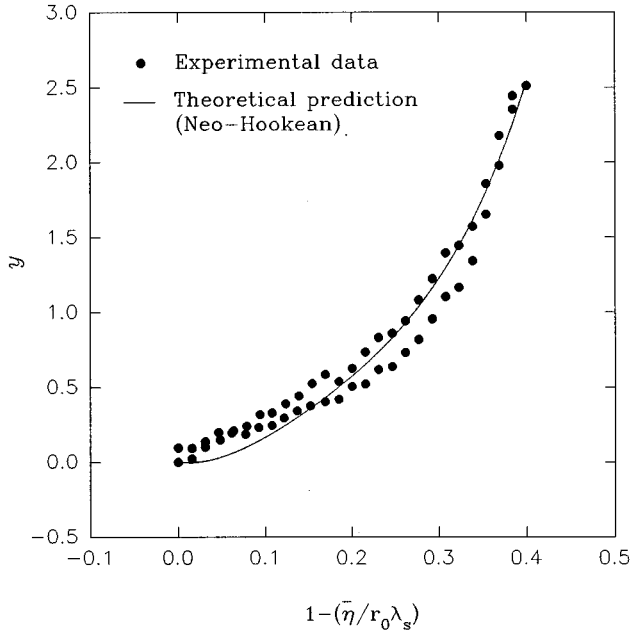

FIG. 7. The dimensionless experimental loading-unloading curve (deformation up to 40%) and theoretical predictions by the membrane model with neo-Hookean material law. The parameter $y=(F/C_1hr_0\lambda_s^2)$ is the dimensionless force and the quantity $1-(\bar{\eta}/r_0\lambda_s)$ is the dimensionless approach. λ_s is 1.0 and C_1 is 16.14 MPa. The wall thickness (h) is taken as 2 μm.

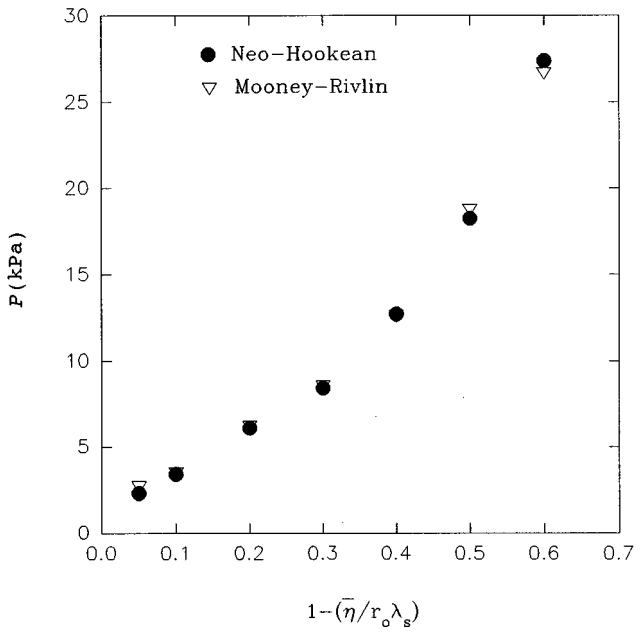

FIG. 8. Internal pressure versus deformation curve of a compressive microcapsule. The assumed Young's moduli of the membrane are, respectively, 2.69 MPa for neo-Hookean material and 2.68 MPa for Mooney-Rivlin material.

very small compared with the corresponding loading value, especially at large deformations. This observation implies that the reflex force contributed by the bending moment of the wall, after rupture, is insignificant during the postrupture deformations and this is consistent with the earlier assumption of a mainly tensile membrane response; that is, the bending contribution is negligible.

Experimental loading-unloading transverse compliance curves are shown in Figs. 6 and 7. In these figures the force F has been nondimensionalized to be in the dimensionless form $y=F/C_1hr_0\lambda_s^2$. The theoretical predications based upon the membrane model with Mooney-Rivlin and neo-Hookean constitutive equations, combined with the minimum least-squares (MLS) fitting to the experimental data, are also shown in Figs. 6 and 7. The extensional rigidity of the membrane, Eh, may be calculated to be 538 N m^{-1} for a neo-Hookean material and 536 N m^{-1} for a Mooney-Rivlin material, respectively, from the MLS fitting between the theoretical predictions and experimental data. The difference is small. Hence if the thickness of the elastomeric membrane wall is assumed to be 2 μm, then the elastic modulus of the membrane can be calculated to be 2.69 MPa for a neo-Hookean material and 2.68 MPa for a Mooney-Rivlin material, respectively. This result, which shows no significant difference between the estimated Young modulus obtained by the Mooney-Rivlin and the neo-Hookean laws, suggests that the second term in the Mooney-Rivlin law, $\beta(I_2-3)$, may not be important for the description of the deformation of these elastomeric membranes. We may also note that a value of the elastic modulus 2.69 MPa is a sensible one for this type of polymeric membrane.

Compared with the experimental data, the theoretical calculation of the loading-unloading curves obtained from the membrane model with either the neo-Hookean material law or the Mooney-Rivlin model are slightly underpredicted when the deformation is below 15%. This difference may arise from the fact that the bending moment still has influence, to some extent, when the deformation is small [11]. For the intact microcapsules the force difference between loading and unloading (shown in Figs. 6 and 7), which is very small, is consistent with the assumption that the transport of encapsulated solution, across the membrane, is insignificant during the chosen time scale of the loading-unloading process. Furthermore, it appears that the viscoelastic effects associated with the deformation of the membrane, again within the chosen time scale, are also negligible. The agreement between theory and experiment, as well as the reasonable prediction of the membrane elasticity, would suggest that the analyses based on both Mooney-Rivlin and neo-Hookean constitutive equations can be generally applied to the compressive deformation of these polymer-bounded microcapsules. Moreover, the close agreement between the theoretical predictions and the experimental loading-unloading curves, as well as the reasonable estimation of the membrane elasticity, would suggest that the analysis based on the membrane model, associated with either the Mooney-Rivlin law or the neo-Hookean constitutive equations, can be applied to the compressive deformation of polymeric membranes.

B. Internal pressure

The computed internal pressure versus deformation curve, which is shown in Fig. 8, indicates a weakly nonlinear increase of the internal pressure with the imposed deformation. This predicted result is important not only for the preservation of the capsule integrity but also for the chemical release

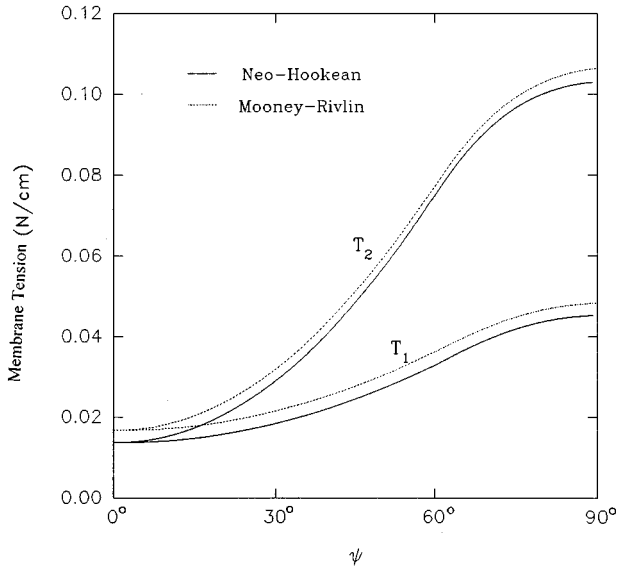

FIG. 9. Variation of the membrane tension with angular position ψ for a 58% deformation; see Fig. 2. The Young's moduli of the membrane are, respectively, 2.69 MPa for neo-Hookean material and 2.68 MPa for the Mooney-Rivlin system. T_1 and T_2 are the stress resultants in the meridional and circumferential directions, respectively.

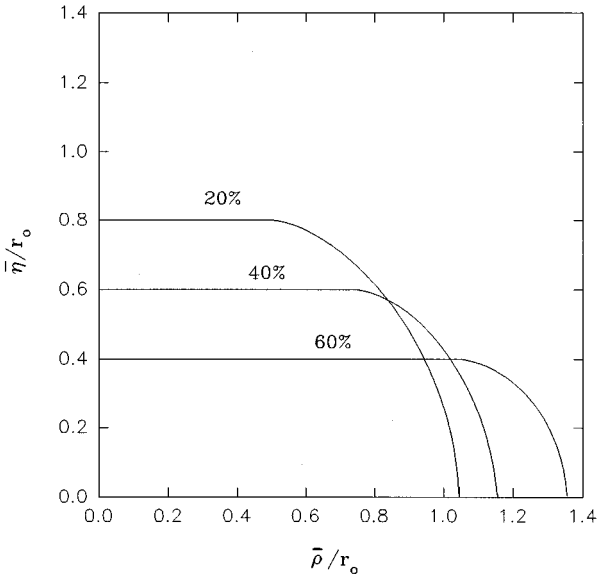

FIG. 10. The simulated deformed shapes of the compressive microcapsule ($\lambda_s=1$, $\beta=0.1$) for 20%, 40%, and 60% deformation in the current study; also see Table I.

behavior of microcapsules. The computed bursting pressure (the pressure at 58% dimensionless approach) is about 26 kPa. This implies a rupture at a nominal membrane strain of about 10% in the radial direction. This rupture strain is rather small for an elastomeric material; a value one order of magnitude greater may have been anticipated. The nature of the preparation of these membranes, a chemical reaction at a liquid-liquid interface, will naturally produce many defects in thickness and composition. Thus while it seems that the membrane is not perfectly porous it may have many thin regions or effective notches which reduce its toughness.

For the modeling of the release rate of encapsulated solutions across the membrane under the deformation, Darcy's law [19], which was derived on the assumption of laminar flow through a cylindrical channel, may be applied to the current case. Basically, this law supposes that the flux of the liquid across a membrane is directly proportional to the pressure difference across the wall, if the membrane is assumed to be a porous medium and the permeability of the membrane a constant. Hence the release rate of the solution for the compressive microcapsules will nonlinearly increase with the deformation due to the nonlinear increase of the internal pressure. The microcapsules used in some applications, such as the time-release drug delivery and for the immobilization of enzymes, are often required to maintain constant release rates of the encapsulated solutions. Therefore the above result is interesting and of crucial value in the control of the performance of such deformed microcapsules.

C. Membrane tension

The membrane tension (the resultant per unit length of the deformed surface) on the membrane can be predicted by the theoretical model. If the elastic modulus of the membrane is 2.69 MPa, the calculated tension profile for the case of a 58% deformation (at rupture) is shown in Fig. 9. The result shows that the tension in the membranes is not uniform but increases with the angular position parameter (ψ). On this basis, the bursting point will always be located on the equator; the compressive loads are imposed from the two parallel plates along the axis of symmetry. This predicted feature is consistent with the experimental observations noted through the image system [see Fig. 5(d)]. This prediction also shows that, for the present case, the resultant stress in the deformed circumferential direction, T_2, is always larger than the stress resultant in the deformed meridional, T_1. The bursting strength, the tension on the equator for 58% deformation, for the microcapsule is computed as about 1.04 N cm^{-1}, which is the stress resultant in the deformed circumferential direction at rupture.

D. Geometric features of the deformation

The simulated deformed external shapes of the microcapsule are shown in Fig. 10. These results show that, for large imposed deformations, the noncontact region must be significantly stretched in order to maintain a constant enclosed volume. The predicted behavior has been identified by measuring the dimensionless central extension [the lateral extended radius of the deformed microcapsule ($\overline{\rho}$) normalized by the initial radius r_0] of the free surface from the microscope images (shown in Fig. 5). The comparison between the values obtained from the experimental measurements and the theoretical predictions is shown in Table I. The results show that the theoretical predictions and the experimental measurement are in good accord.

The contact area measurement has been a key experimental variable used in the evaluation of the theories. Though the measurement of the area of contact has been proven to be viable in large scale macroscopic experiments, it has proven to be far more difficult at the microscopic scale. Due to the diffraction limit, the resolution of conventional optical systems is, at best, 0.25 μm. However, practically it can often

TABLE I. The comparison of the experimental and theoretical dimensionless central laternal extension versus dimensionless approaches.

Dimensionless approach (%)	Dimensionless central laternal extension	
	Theoretical prediction	Experimental measurements
20	1.045	1.056±0.008
40	1.150	1.152±0.010

be difficult to resolve dimensions of less than 1 μm and other workers have also noted that the precise measurement of the contact area for microscopic systems has proven to be intractable [20]. In the current case, for a 65 μm microcapsule, at 20% deformation, the radius of the contact area is about 16 μm according to the theoretical prediction (Fig. 10). Hence the resolution of optical system would result in an error possibly as large as about 6%. Yoneda [10] has attempted to directly measure the contact area of compressed sea-urchin eggs (about 120 μm) between two plates by the use of photomicrographs taken from the side view. He pointed out that it would be nearly impossible to detect a very narrow gap between the egg and the plate, using optical methods, and this would cause a major overestimation of the area of contact. Of course, these measurements may be accurately resolved by a new method; for example, x ray imaging is a possibility.

V. CONCLUSIONS

A model to describe the deformation of a liquid-filled spherical elastic membrane microcapsule with either a Mooney-Rivlin law or a neo-Hookean constitutive equation has been verified. This model allows correlations to be made using the experimental microcompression data provided for the determination of the elasticity and the tension distribution and bursting strength of the membrane as well as the pressure difference across the membrane. The feature where the internal pressure nonlinearly increases with the compressive deformation may be an extremely important result for the usage of microcapsules as drug, or active species, delivery systems. The characterization of the major geometric deformational parameters has been made, and provides a confirmation of the predictive capacity of the theoretical model.

ACKNOWLEDGMENTS

The authors are grateful for the financial support provided by the DTI initiative in ''Colloid Technology.'' We also acknowledge D. J. Brown (Zeneca) for the provision of microcapsules and Dr. P. F. Luckham for many useful discussions. K. K. L. would like to thank the Taiwanese government for the provision of financial support.

[1] T. Loftsson and T. Kristmundsóttir, in *Polymeric Delivery Systems—Properties and Applications*, edited by M. A. El-Nokaly, D. M. Piatt, and B. A. Charpentier, ACS Symposium Series Vol. 520 (American Chemical Society, Washington, DC, 1993).
[2] I. Jalsenjak, C. T. Nicolaidou, and J. R. Nixon, J. Pharm. Pharmacol. **28**, 912 (1976).
[3] W. Prapaitrakul and C. W. Whitworth, Drug Dev. Ind. Pharm. **16**, 1427 (1990).
[4] D. Halpern and T. W. Secomb, J. Fluid Mech. **244**, 307 (1992).
[5] A. W. L. Jay and M. A. Edwards, Can. J. Physiol. Pharmacol. **46**, 731 (1968).
[6] K. S. Chang and W. L. Olbricht, J. Fluid Mech. **250**, 587 (1993).
[7] Z. Zhang, R. Saunders, and C. R. Thomas, Inst. Chem. Eng. Res. Event **2**, 722 (1994).
[8] W. W. Feng and W. H. Yang, J. Appl. Mech. **40**, 209 (1973).
[9] T. J. Lardner and P. Pujara, in *Mechanics Today*, edited by S. Nemat-Nasser (Pergamon, New York, 1980), Vol. 5.
[10] M. Yoneda, Adv. Biophys. **4**, 153 (1973).
[11] L. A. Taber, J. Appl. Mech. **49**, 121 (1982).
[12] D. R. Williams, K. K. Liu, and B. J. Briscoe, Rev. Sci. Instrum. (to be published).
[13] D. J. Brown, B. J. Briscoe, and P. F. Luckham, J. Colloid Interface Sci. (to be published).
[14] Y. C. Fung, *Biomechanics*, 2nd ed. (Springer-Verlag, New York, 1993).
[15] M. Mooney, J. Appl. Phys. **11**, 582 (1940).
[16] R. S. Rivlin, Philos. Trans. R. Soc. London, Ser. A **241**, 379 (1948).
[17] A. E. Green and J. E. Adkins, *Large Elastic Deformation*, 2nd ed. (Oxford University Press, New York, 1970).
[18] J. H. Ferziger, *Numerical Methods for Engineering Application* (Wiley, New York, 1981).
[19] H. Darcy, *Les Fontaines Publiques de la Vill de Dijon* (Dalmont, Paris, 1856).
[20] E. A. Evans and R. Skalak, *Mechanics and Thermodynamics of Biomembranes* (CRC Press, Boca Raton, 1979).